



Universidad Autónoma  
de Madrid



Repositorio Institucional de la Universidad Autónoma de Madrid

<https://repositorio.uam.es>

Esta es la **versión de autor** del artículo publicado en:

This is an **author produced version** of a paper published in:

Chemical Engineering Journal 405 (2021): 127016

**DOI:** <https://doi.org/10.1016/j.cej.2020.127016>

**Copyright:** © 2020 Elsevier B.V. This manuscript version is made available under the CC-BY-NC-ND 4.0 licence <http://creativecommons.org/licenses/by-nc-nd/4.0/>

El acceso a la versión del editor puede requerir la suscripción del recurso

Access to the published version may require subscription

# Removal of Pemetrexed from aqueous phase using activated carbons in static mode

Bomin Fu <sup>a</sup>, Corinne Ferronato <sup>a,\*</sup>, Ludovic Fine <sup>a</sup>, Frederic Meunier <sup>a</sup>, Jose Luis Valverde <sup>b</sup>,  
Victor R. Ferro Fernandez <sup>c</sup>, Anne Giroir-Fendler <sup>a</sup>, Jean-Marc Chovelon <sup>a,\*</sup>

<sup>a</sup> Univ. Lyon, Université Claude Bernard Lyon 1, CNRS, IRCELYON, 2 avenue Albert Einstein, F-69626, Villeurbanne, France

<sup>b</sup> Department of Chemical Engineering, University of Castilla La Mancha, Avda. Camilo José Cela 12, 13071, Ciudad Real, Spain

<sup>c</sup> Dpto. Ingeniería Química. Univ. Autónoma de Madrid. 28049 Madrid, Spain

\* Corresponding author.

E-mail address: corinne.ferronato@ircelyon.univ-lyon1.fr

E-mail address: jean-marc.chovelon@ircelyon.univ-lyon1.fr

## **Abstract**

Three activated carbons (ACs) obtained from wood and activated either by steam (AC1) or phosphoric acid (AC2, AC3) were characterized *via* nitrogen adsorption–desorption isotherms, zeta potentials, infrared and Raman spectroscopy, as well as their chemical analysis was determined. Adsorption experiments with Pemetrexed (PEME), a pharmaceutical used for the treatment of tumors, were carried out in which adsorbent doses, contact times, temperatures, and solution pH were investigated. Correlation between the physicochemical properties of ACs and the adsorption capacity was proposed.

According to the results, it was found that AC1 and AC3 were better described by the Freundlich and Langmuir models, respectively, whereas both models could be used to fit the adsorptive isotherm of AC2. The higher the initial PEME concentration or the temperature, the higher the adsorption capacity was. The adsorption capacities of the adsorbents were in the following order,  $AC3 > AC2 > AC1$ , in agreement with their specific surface areas. A coexistence process of physical and chemical adsorption existed in all ACs as predicted by the best fitting obtained with the Dubinin–Radushkevich, pseudo–second–order kinetic and Elovich models.

The adsorption mechanisms were researched using the Conductor–like Screening Model methodology to determine the proton donor and acceptor centres in PEME. As main conclusion, supported by DRIFTS analysis and O/C ratios, AC3 and AC2 containing more oxygenated groups, must adsorb PEME onto their surface according to a monolayer adsorption mechanism. Fitting procedure demonstrated that the equilibrium data obtained with these two materials can be fitted to the Langmuir isotherm.

## **Keywords:**

Pemetrexed; Activated carbon; Characterization; Polarized charge distribution; Adsorption mechanism

## 1. Introduction

Water is not only an essential element for human beings but also an important factor in social and economic processes. However, water availability is threatened in recent years because of an increase in anthropogenic pollutants from the non-industrial and industrial sectors [1]. Approximately two million tons of wastewater is being discharged into freshwater every day [1]. In particular, conventional wastewater treatment plants (WWTPs) are not specifically designed to efficiently remove residual concentrations of bioactive compounds such as pharmaceutical ones [2]. As a consequence, a lot of these compounds are directly discharged into natural water contributing to new environmental issues. An effective process for removing these contaminants should be the addition of a tertiary treatment in WWTPs. Various technologies have been extensively developed and used in this context, such as precipitation, oxidation, membrane filtration, reverse osmosis, evaporation, ion exchange and adsorption [3,4]. Among these different potential treatments, adsorption represents a promising and effective method, owing to its numerous advantages such as ease of implementation, relatively low cost, no addition and use of chemical products, and no generation of harmful by-products [5].

Activated carbon (AC) is a typical adsorbent obtained by carbonization of practically any carbonaceous material. The use of cheap and renewable raw materials (e.g. wood) as precursors not only reduces the production cost of AC but also limits the problems of environmental pollution caused since these raw materials are usually waste ones. Besides the carbonization process, an activation step involving chemical and/or physical methods, is required to further generate a structure with abundant pores. On the other hand, the gasification process using steam is an effective procedure for producing high surface area AC due to the favorable effect of the diffusion of smaller water molecules within the porous

structure of the precursor [6]. Additionally, a previous study has shown that activated carbons with high apparent pore volume and surface areas were obtained by treating the endocarp of babassu coconut with phosphoric acid during the chemical activation procedure [7]. AC is used to eliminate contaminants from water relies mainly on its high specific surface area, well-developed pore structure, large pore volume as well as surface properties [8,9]. For example, Baccar et al. used a homemade AC activated by phosphoric acid for the elimination of pharmaceutical compounds at a laboratory scale [10]. The adsorption capacities based on the Langmuir model were 56, 11, 25 and 40 mg.g<sup>-1</sup> for diclofenac, ibuprofen, ketoprofen and naproxen, respectively, under the conditions of original solution pH 4 at 25 °C for 26 h. The adsorption characteristics of trimethoprim from aqueous solution onto a powdered AC from wood were investigated by Kim et al [11]. The experimental data is in good agreement with the Langmuir model; the maximum adsorption capacity calculated from the model was 258 mg.g<sup>-1</sup> for AC. Kleywegt et al. reported that the use of granulated AC could increase the removal efficiency of carbamazepine from 71 to 93% for water treatment in Ontario, Canada [12].

Pemetrexed (PEME) is a novel generation of anti-folate pharmaceutical showing encouraging activity in the treatment of a variety of tumors, e.g., malignant mesothelioma, non-small cell lung cancer, breast cancer, bladder cancer, colorectal carcinoma and cervical cancer [13]. Consequently, PEME consumption increases year by year, especially in European countries and it is worth noting that PEME environmental concentrations in France for years 2004 and 2008 were reported to be 0.02 and 0.85 ng.L<sup>-1</sup>, respectively [14]. Additionally, it is estimated that ca. 78% of residual PEME is continuously released into the surface water from WWTPs due to its own characteristics (water-soluble, non-volatile and weakly metabolized) [15]. At the same time, its intended function may cause potential risks,

including genotoxic, mutagenic, cytotoxic effects to aquatic organisms, which represents a new challenge to be solved [15].

To the best of our knowledge, there is currently no systematic study on the removal of PEME from water by any type of adsorbent. Considering the potential advantages of AC, it can be selected as a sorbent material to remove PEME. In this study, the adsorption behavior of PEME in water by different types of ACs was investigated. The main purposes of this article were to explore the effects of different factors such as the adsorbent dose, contact time, pollutant concentration, temperature and pH conditions on the adsorption of PEME to determine the best materials and experimental conditions for removing PEME from water. In addition, the adsorption mechanisms were researched using the Conductor-like Screening Model (COSMO) methodology in a computational procedure to determine the proton donor–acceptor centres and the polarized charge distribution in PEME. Finally, Raman spectrometry was carried out to assess the  $\pi$ – $\pi$  interactions between PEME and ACs.

## **2. Materials and methods**

### *2.1. Materials*

Pemetrexed disodium heptahydrate (CAS No. 357166–29–1) was purchased from Sigma–Aldrich. The physicochemical properties of PEME are listed in Table S1. Deionized water was prepared from a Millipore Milli–Q system (18.2 M $\Omega$  cm). High–performance liquid chromatography (HPLC) grade methanol was supplied by Carlo Erba Reagents. Other chemical reagents used in the work were of analytical grade.

Three commercial ACs powders produced from wood and activated either by steam (AC1) or H<sub>3</sub>PO<sub>4</sub> (AC2, AC3) were selected for this study. AC1 and AC3 were supplied by Oxbow whereas AC2 was manufactured by Cabot.

## 2.2. Characterizations of ACs

Pore structure characteristics of ACs were measured by adsorption–desorption isotherms at  $-196\text{ }^{\circ}\text{C}$  using a 3FLEX Micromeritics instrument. Before the measurement, the samples were pretreated by degassing at  $300\text{ }^{\circ}\text{C}$  for 1 h in a vacuum condition. Brunauer–Emmett–Teller (BET) standard equation was used to estimate the specific surface area in the sample. Microporous surface areas and pore volumes of ACs were derived from the t-Plot method, and the median pore width obtained by using Horvath–Kawazoe (H–K) model. Mesoporous volumes and average pore diameters of samples were calculated *via* Barrett–Joyner–Halenda (BJH) method.

Total C, O, H, N and S contents in the ACs were determined by an elemental analyzer (Vario EL cube, Germany). A Plasma Optical Emission Spectrometer (ICP–OES, HORIBA Jobin Yvon–ACTIVA) was used for the analysis of the other elements. Prior to analysis, a part of the sample was attacked with  $\text{H}_2\text{SO}_4 + \text{HNO}_3$  at  $250\text{--}300\text{ }^{\circ}\text{C}$  to detect the contents of P, Fe, Na, Al, Mg, K, Mo, Mn, Zn, whereas for Ca and Ba, samples were dissolved by  $\text{HClO}_4 + \text{HNO}_3$  at  $250\text{--}300\text{ }^{\circ}\text{C}$ . Regarding the following atoms, Si, Ag, As, Cd, Co, Cr, Cu, Ni, Pb, Sb, Se, Ti, Tl, V, Zr, Sr, Te, Bi, Ga, In, Ta and Hf, the samples were first melt etched with lithium tetraborate and then heated in a muffle furnace until  $1100\text{ }^{\circ}\text{C}$  with 20% HCl.

The pH values of each solution were determined using a PHM 210 Standard pH meter (Radiometer) connected to a combined glass electrode. The zeta potentials were measured using a CAD ZetaCompact instrument for the detection of electrophoretic mobility of ACs particles in aqueous suspensions.

The IR data were collected in the diffuse reflectance mode (DRIFTS) using a Spectra–Tech® reaction cell fitted with KBr windows. The cell was located in a Collector™ assembly placed in a Nicolet 570 spectrometer. A liquid– $\text{N}_2$  cooled MCT detector was used. A

description and properties of the cell can be found elsewhere [16]. DRIFTS spectra were recorded at a resolution of  $4\text{ cm}^{-1}$  and 32 scans were averaged. A reference signal was collected over KBr, from which the pseudo-absorbance  $\text{Log}(1/R)$  was calculated, where R is the sample reflectance with respect to the KBr reference [17].

The Raman spectra of the samples were tested *via* a Horiba Jobin–Yvon Raman instrument equipped with a  $\times 50$  objective at 514 nm excitation wavelength, 1800 grating lines/mm, and 20 seconds exposure time for 5 accumulations.

### 2.3. Adsorption experiments

Batch adsorption experiments were performed using 50 mL centrifuge tubes. Each tube contained a 40 mL PEME solution and different ACs loads. The tubes were shaken at a constant speed of 200 rpm in a mechanical shaker and after sorption experiments, the samples were filtered using  $0.45\text{ }\mu\text{m}$  PVDF filters. The residual concentration of PEME in the filtrate was then determined using HPLC and no loss of PEME from the centrifuge tubes was observed during the sorption process carried out without ACs.

For the adsorbent dose experiments, PEME solutions at a concentration of  $10\text{ mg.L}^{-1}$  were mixed with different ACs doses ( $0.0125$ ,  $0.025$ ,  $0.0375$ ,  $0.05$ ,  $0.0625$  and  $0.075\text{ g.L}^{-1}$ ) and then shaken for 24h at  $25\text{ }^{\circ}\text{C}$ . The pH of all the solutions was not adjusted during the course of the reaction.

Isotherm experiments: samples (pH not adjusted) containing different PEME concentrations and  $0.0375\text{ g.L}^{-1}$  of ACs were shaken at  $15$ ,  $25$ , and  $35\text{ }^{\circ}\text{C}$ , respectively, until equilibrium was reached. In order to better shed light to the adsorption mechanism of PEME onto the different adsorbents, PEME concentrations of  $2$ ,  $5$ ,  $10$ ,  $15$ , and  $20\text{ mg.L}^{-1}$  were selected for the study.



Kinetic experiments: samples (pH not adjusted) that contained an initial PEME concentration of  $10 \text{ mg.L}^{-1}$  and  $0.0375 \text{ g.L}^{-1}$  of ACs were shaken at the desired time intervals of 0.5, 1, 2, 4, 8, 12, 24, 30, 36, 42 and 48 h at  $25^\circ\text{C}$ .

The influence of the solution pH: different values of initial pH of PEME solutions were adjusted by the addition of 0.1, 0.5, 1 M HCl and/or NaOH. Samples containing  $10 \text{ mg.L}^{-1}$  PEME and  $0.0375 \text{ g.L}^{-1}$  of ACs with different initial pH were shaken at  $25^\circ\text{C}$  until equilibrium was reached.

All the adsorptive experiments were performed three-fold; the results were shown as means and standard deviations.

#### *2.4. Analytical methods*

The concentration of PEME in water was determined through a PerkinElmer Flexar HPLC coupled with an UV/Vis detector. Samples were separated by a C18 Column (4 x 125 mm,  $5 \mu\text{m}$ ). Mobile phase consisted of 30% methanol and 70%  $0.005 \text{ mol/L NaH}_2\text{PO}_4$  (pH = 5.0) at a flow rate of  $0.5 \text{ mL.min}^{-1}$ . Injection volume was fixed to  $20 \mu\text{L}$  and detection wavelength for PEME was selected at 226 nm.

#### *2.5. Computational procedure*

Molecular geometries of PEME were optimized using the functional B3LYP and 6-31G (d, p) atomic basis considering isolated molecules. Gaussian v16-c01 program package was employed for geometry optimizations. Afterwards (on the previously optimized structures), continuous solvation single point calculations were performed by the COSMO methodology aiming to establish the polarized charge density distribution on the PEME surface. COSMO calculations were carried out with the functional BP86 and TZVPD atomic basis in Turbomole v7.1. So as to improve the quality of the COSMO calculations, the algorithm

FINE recently implemented in Turbomole was used to create the solvent cavity. The pKa calculations were done by COSMO–RS method performed with the COSMOthermX v19.0 program package using the BP\_TZVPD\_FINE\_19 parametrizations to elucidate the PEME structure under different pH conditions.

## 2.6. Equations used

Adsorbent dose is one of the main factors that can affect the sorption efficiency of PEME. The removal rate ( $R$ , %) of PEME by ACs was calculated based on the following equation (Eq.1):

$$R(\%) = \frac{C_0 - C_e}{C_0} \times 100 \quad (1)$$

where  $C_0$  (mg.L<sup>-1</sup>) and  $C_e$  (mg.L<sup>-1</sup>) are the PEME concentration at initial and equilibrium time, respectively.

The adsorption capacities of PEME on ACs were quantified by using the following equation (Eq.2):

$$q = \frac{m}{V} \quad (2)$$

where  $q$  (mg.g<sup>-1</sup>) is the adsorption capacity of ACs,  $V$  (L) is the volume of PEME solution, and  $m$  (g) is the mass of ACs.

Three models were used for fitting the adsorption equilibrium data: Freundlich (Eq.3), Langmuir (Eq.4) and Dubinin–Radushkevich (Eq.5) [18,19]:

$$q = K_f C_e^{1/n} \quad (3)$$

$$q = \frac{q_m C_e}{K_L + C_e} \quad (4)$$

$$q = q_m \exp\left(-\frac{A}{2B}\right) \quad (5)$$

$$q_e = \frac{K_F C^n}{1 + K_F C^n} \quad (2)$$

where  $q_e$  (mg.g<sup>-1</sup>) is the adsorption capacity at equilibrium,  $n$  (dimensionless) is the Freundlich index for heterogeneity,  $K_F$  (L.g<sup>-1</sup>) is the Freundlich coefficient associated to the adsorption capacity,  $q_m$  (mg.g<sup>-1</sup>) is the maximum monolayer adsorption capacity,  $K_L$  (L.mg<sup>-1</sup>) is the Langmuir coefficients related to the adsorption energy,  $q_{mD}$  (mg.g<sup>-1</sup>) is the maximum adsorption capacity estimated from Dubinin–Radushkevich model,  $K_D$  (mol<sup>2</sup>.kJ<sup>-2</sup>) is a constant related to the mean free energy of adsorption,  $R$  (8.314 J.(mol.K)<sup>-1</sup>) is the gas constant, and  $T$  (K) is the absolute temperature. Mean free energy  $E$  (kJ.mol<sup>-1</sup>) was calculated by using Eq.6. Non-linear analysis based on the Levenberg–Marquardt algorithm and determination coefficients ( $R^2$ ) was conducted by Origin version 9.0 software (OriginLab, USA).

The surface density ( $d_{sur}$ ) is a valuable parameter to understand the interaction between PEME molecules and the surface of ACs. It was estimated by the next equation [20,21]:

$$d_{sur} = \frac{q_m \cdot M}{S_{BET} \cdot N_A} \quad (3)$$

where  $q_m$  (mg.g<sup>-1</sup>) is the maximum adsorption capacity estimated from the Langmuir model,  $m$  (g) is the mass of ACs used,  $M$  (g.mol<sup>-1</sup>) is the molecular mass of PEME,  $N_A$  is the number of Avogadro (6.02×10<sup>23</sup> mol<sup>-1</sup>), and  $S_{BET}$  (m<sup>2</sup>.g<sup>-1</sup>) is the BET surface area.

For better understanding the characteristics and mechanisms of sorption kinetics of PEME onto ACs, the experimental data were analyzed by a pseudo-first-order-model (Eq.8), a pseudo-second-order model (Eq.9), the Elovich model (Eq.10) and an intra-particle diffusion model (Eq.11) [22]:

$$q_t = q_e (1 - e^{-k_1 t}) \quad (4)$$

$$q_t = \frac{k_2 q_e^2 t}{1 + k_2 q_e t} \quad (5)$$

$$q_t = \frac{q_{\infty}}{1 + \frac{k_2}{k_1} \exp(-k_1 t)} \quad (1)$$

$$q_t = \frac{q_{\infty}}{1 + \frac{k_2}{k_1} \exp(-k_1 t)} \quad (2)$$

where  $t$  (h) is the adsorption time,  $q_t$  (mg.g<sup>-1</sup>) is the adsorption capacity at  $t$ ,  $k_1$  (h<sup>-1</sup>) is the adsorption rate constant of the pseudo-first-order kinetic,  $k_2$  (g.(mg.h)<sup>-1</sup>) is the adsorption rate constant of the pseudo-second-order kinetic,  $\alpha$  (mg.(g.h)<sup>-1</sup>) is a constant associated to chemisorption rate,  $\beta$  (g.mg<sup>-1</sup>) is an indicator of desorption,  $k_d$  (mg.(g.h<sup>0.5</sup>)<sup>-1</sup>) an intra-particle diffusion rate constant and  $C$  (mg.g<sup>-1</sup>) is a constant linked with the thickness of the boundary layer. All the parameters of the kinetic models and  $R^2$  were evaluated by Origin 9.0.

Two types of acid–base equilibria involving PEME were considered:



(1)



(2)

The acidic pKa values were calculated by COSMO–RS. The acidic equilibrium constant  $K_{eq(a)}$ , pKa and the basic equilibrium constant  $K_{eq(b)}$  were obtained from Eq. (14), Eq. (15) and Eq. (16), respectively:

$$K_{eq(a)} = \frac{[\text{PEME}][\text{H}_3\text{O}^+]}{[\text{PEME}][\text{H}_2\text{O}]}$$

$$K_{eq(b)} = \frac{[\text{PEME}^+][\text{OH}^-]}{[\text{PEME}][\text{H}_2\text{O}]}$$

$$pK_a = -\log K_{eq(a)}$$

$$pK_b = -\log K_{eq(b)}$$

$$pK_a = -\log K_{eq(a)}$$

$$pK_b = -\log K_{eq(b)}$$

The graphitization degree of ACs determined by Raman spectroscopy can be assessed using the following equation [23]:

where  $R$  represents the graphitization degree of ACs.  $I_D$  and  $I_G$  are the intensities of the D and G bands in the Raman spectra, respectively. The smaller the  $R$  value, the higher the degree of graphitization is, which would indicate that the surface of the AC contains a great amount of graphite-like domains facilitating the stacking interactions between the adsorbate and the adsorbent [23,24].

### 3. Results and discussion

#### 3.1. Characterizations of ACs

The International Union of Pure and Applied Chemistry (IUPAC) classifies porous substances into three categories depending upon their pore diameters:  $< 2$  nm is micropore, 2–50 nm is mesopore,  $> 50$  nm is macropore [25]. The  $N_2$  adsorption–desorption isotherms of ACs (Fig. S1) exhibited a type I isotherm with a slight hysteresis loop for AC1, and a IV type isotherm with H4-shaped hysteresis loop for AC2, as well as a type IV isotherm with H3 hysteresis loop for AC3 according to the IUPAC classification [26]. This would indicate that AC1 possessed wider micropores and narrower mesopores whereas both AC2 and AC3 presented a broad distribution of micropores and mesopores, as also revealed by their pore size distributions shown in Fig. S2 and Fig. S3. The textural properties of ACs are presented in Table 1. The  $S_{BET}$  ( $1721 \text{ m}^2.\text{g}^{-1}$ ),  $S_{micro}$  ( $994 \text{ m}^2.\text{g}^{-1}$ ),  $V_{meso}$  ( $1.30 \text{ cm}^3.\text{g}^{-1}$ ),  $V_{micro}$  ( $0.51 \text{ cm}^3.\text{g}^{-1}$ ),  $W_{micro}$  (1.26 nm) and  $D_{meso}$  (4.93 nm) of AC3 are higher than those of the other two ACs.

Table 2 lists the total amount of C, O, H, N, and S as well as the elemental ratios (O/C, (O+N)/C) used to estimate the polarity in AC [27]. AC1 contains the highest C (86.3%) content and the lowest contents of O (5.7%) and H (1.0%), showing the lowest polarity:

(O+N)/C ratio of 0.07. Both AC2 and AC3 have higher O content and higher values of O/C and (O+N)/C ratios, which would indicate the major presence of O-containing functional groups on their surfaces.

Table 3 shows the content of other elements in ACs. It can be seen that AC1 contains more inorganic species: Fe, Ca, Na, Al, Mg, K, Si and, especially, Ca with a content of ca. 1.5%. On the other hand, the P content is higher in both AC2 and AC3 than in AC1, which is associated to the activation method followed in the preparation of the formers based on the use of H<sub>3</sub>PO<sub>4</sub>. Nonetheless, the presence of Ag, As, Cd, Co, Cr, Cu, Ni, Pb, Sb, Se, Ti, Tl, V, Zr, Sr, Te, Bi, Ga, In, Ta and Hf in all ACs were considered to be as negligible.

The zeta potential at different pH was investigated and the results are presented in Fig.1. Clearly, the zeta potentials for all ACs decreased when the pH increased from 3 to 10. The pH corresponding to the point of zero charges (pH<sub>pzc</sub>) deduced from the curves was 3.5, 3.6 and 4.5, for AC1, AC2 and AC3, respectively. Hence, the surfaces of ACs were negatively charged above their pH<sub>pzc</sub>, and positively charged at lower pH values.

DRIFTS spectra are displayed in Fig. 2. They were collected at 100 °C under a He stream to remove most of adsorbed water that was present at room temperature (data not shown). The spectrum of AC1 is essentially featureless, probably due to a low content of functionalized groups, although a low depth of penetration of the beam into this sample cannot be excluded. In contrast, AC2 and AC3 exhibited several strong bands assigned to C=O (1596 and 1706 cm<sup>-1</sup>) and C–O (1265 and 1435 cm<sup>-1</sup>) vibrations [28]. Bands due to P–O stretching vibrations, typically located between 1200 and 800 cm<sup>-1</sup> [29] were likely present but they cannot be discriminated from those of C–O bonds. The presence of bands associated to the presence of oxygenated groups on the AC2 and AC3 samples was consistent with their higher oxygen content if compared to that of AC1 (Table 2).

The broad band spanning over 3700–2700  $\text{cm}^{-1}$  for the AC2 sample was attributed to H-bonded hydroxyl stretching vibration. Such hydroxyl groups can belong to carboxylic or phenolic group. Since AC2 also presented a strong band at 1706  $\text{cm}^{-1}$ , usually assigned to carboxylic acidic groups, one can claim that AC2 contained more acidic groups than AC3. This finding was in line with the zeta potential results obtained at pH higher than 5. Bands at 3060  $\text{cm}^{-1}$  were also observed, which were assigned to vibrations of C–H in aromatic groups.

### 3.2. *Effect of adsorbent dose*

The effect of adsorbent dose on PEME removal is depicted in Fig. 3. The results show that the  $R$  of PEME increased as the ACs dose raised from 0.0125 to 0.075  $\text{g.L}^{-1}$  due to the increase in total number of available adsorptive sites in the solid–liquid system. Nevertheless, the  $R$  of PEME for AC3 increased slowly beyond 0.0375  $\text{g.L}^{-1}$ , probably due to an aggregation of available binding sites through the functional groups interactions between the particles in the presence of excess ACs, resulting in a large amount of adsorbed unoccupied surface area [30,31].

### 3.3. *Adsorption isotherm*

The adsorption capacity of PEME onto ACs at different temperatures ranging from 10 to 35 °C is depicted in Fig. 4. It can be clearly observed that the adsorbed amount at equilibrium increased as the initial concentration of PEME increases from 2 to 20  $\text{mg.L}^{-1}$  [6]. Temperature was also an important factor affecting the adsorption process of organic compounds from liquid phase onto adsorbent. The results also showed that an increase in temperature favored the PEME adsorption capacity on the three ACs. However, the results obtained at 25 and 35 °C are relatively close. Fig. 4 shows different isotherm trends between AC3 and AC1/AC2, which could be associated to the structure of the adsorbents. AC3 has

the highest  $W_{\text{micro}}$  and  $D_{\text{meso}}$  (cf. Table 1), which may allow adsorbate molecules to enter the sorbent pores more easily.

Freundlich model assumes a heterogeneous surface in the adsorbent as well as multilayer adsorption with non-uniform energy distribution of active sites along with interactions between adsorbed substances [19]. Regarding the Langmuir isotherm model, the maximum adsorption capacity is evaluated by assuming that a monolayer adsorption occurs at definite homogeneous active sites within the adsorbent, and that there are no interactions between adsorbates even at adjacent sites [32]. The Dubinin–Radushkevich isotherm equation which is based on the adsorption potential theory of Polanyi was used to analyze the characteristic porosity of ACs and evaluate the mean free energy used in the adsorption process [19].

Table 4 shows all the calculated parameters from the three isotherm models. None of them can be used to fit correctly the experimental data for all ACs. Regardless the tested temperature, equilibrium data obtained with AC1 was better fitted by the Freundlich isotherms ( $R^2 > 0.99$ ), which may reflect a preference for a multilayer adsorption of PEME on the surface of this AC. Regarding AC2, both Freundlich and Langmuir models fit in a similar way the experimental data. Finally, the Langmuir model provides higher values of  $R^2$  than the Freundlich one for AC3. In addition, it can be pointed out that the values of experimental maximum adsorption capacities for PEME deduced from Fig. 4, agreed well with the trend of  $q_m$  values computed from the Langmuir model. It was observed that the fitting of the experimental data to the Dubinin–Radushkevich model presented relatively high  $R^2$  values. The mean free energy  $E$  deduced from this model for all samples was in the range of 2.4–3.4  $\text{kJ.mol}^{-1}$ , indicating a physisorption process ( $E < 8 \text{ kJ.mol}^{-1}$ : physical adsorption;  $E = 20\text{--}40 \text{ kJ.mol}^{-1}$ : chemical adsorption) [33].



The values of  $q_m$  obtained from Langmuir model at 25 °C (Table 4) were used to calculate the surface density,  $d_{\text{sur}}$ , yielding values for AC1, AC2 and AC3 of 0.239, 0.230 and 0.265 molecule.nm<sup>-2</sup>, respectively. Since these values do not follow the same trend of values of  $q_m$  for the three ACs (cf. Table 4), it would mean that the adsorption process also depended on the presence of surface functional groups.

It is well known that the adsorption is an exothermic process [23,34,35]. However, the results presented here showed that adsorption capacity increases with increasing temperature, which could be associated to a more complex mechanism. In fact, the adsorption behavior in aqueous phase was affected not only by conventional adsorbate–adsorbent interactions, but also by adsorbate–solvent interactions [36,37]. For example, if adsorbates are prone to give strong H bonding with solvent, the increase in temperature will weaken H–bond interactions, and then an endothermic dehydration of the adsorbate takes place. Furthermore, a swelling effect in the internal structure of ACs may occur at high temperatures, allowing PEME molecules to further penetrate into the pores of the adsorbent, thus enhancing the adsorption capacity [32].

### 3.4. Adsorption kinetics

The effect of contact time on PEME adsorption onto ACs is shown in Fig. 5. The order of adsorption capacities ( $q_t$ ) was as follows: AC3 > AC2 > AC1. Regarding the different curves, it can be observed that the adsorption processes can be divided into two steps: a pronounced step in which 67%, 69% and 83% of PEME adsorption capacities were reached after four hours for AC1, AC2, AC3, respectively, followed by a slower evolution until the adsorption equilibriums were reached after ca. 30 h for AC3, and 36 h for both AC1 and AC2.

The values of the parameters of the kinetic models and  $R^2$  are summarized in Table 5. The comparison of the  $R^2$  obtained using the pseudo–first–order and the pseudo–second–

order models for all ACs (0.7530–0.9074 vs. 0.8534–0.9944) suggests that the kinetic data were better described by the latter. This fact would indicate that chemisorption may be one of the adsorption mechanisms between PEME and ACs [38]. These results together with the fact that experimental data were adequately fitted to the Dubinin–Radushkevich model suggests that the interaction between ACs and PEME should involve the occurrence of simultaneous physical and chemical adsorption phenomena. Additionally, the adsorption capacities at equilibrium  $q_e$  estimated by the pseudo–second–order model (cf. Table 5) are more consistent with the experimental data deduced from equation 2 in which the following values were obtained: 109, 167 and 229 mg.g<sup>-1</sup> for AC1, AC2 and AC3, respectively. The Elovich model, which considers that the solid surface is energetically heterogeneous, can be used to describe the chemisorption process. It can be observed that sample AC3 owned the highest value of  $\beta$ , which would indicate the impact of the chemisorption process of PEME onto it. On the other hand, sample AC1 presented the highest value of  $\alpha$ , which could be associated a more effective interaction with PEME and a relatively stronger irreversibility in the adsorption process [39].

Weber and Morris found that the solute uptake onto adsorbent almost varies proportionally with  $t^{0.5}$  rather than with the contact time  $t$  during the adsorption process [40]. Thus, to explore the rate–limiting step of the entire adsorption process, the Weber–Morris plot of  $q_t$  versus  $t^{0.5}$  was considered and is displayed in Fig. 6. Obviously, the plots show multi–linearity for all ACs, indicating that more than one rate–limiting step controls the adsorption of PEME [41]. The first straight portion corresponds to a fast step that was mainly attributed to solute molecules transfer through the film diffusion to the sorption sites on the external surface of adsorbents. Subsequently, a slow stage represented by a second beeline occurred in the adsorption process due to the rate–limiting dependence on the intra–particle diffusion of PEME into the pores and channels of ACs. Indeed, by looking at Table 5, the

high  $R^2$  values suggest that the intra-particle diffusion model better fitted with the experimental results of the second portion. Considering the parameters of the intra-particle diffusion model, the highest  $C$  value obtained for AC3 would indicate a thicker boundary layer with a greater limiting effect surely due to its larger pore volume (cf. Table 1). However, its  $k_d$  for which the value is between the ones of AC1 and AC2 seems to indicate different characteristics inside the interior pore structure [39]. It is worth noting that the lowest  $k_d$  value appeared on AC1 because of its smallest mesopore volume, and average pore diameters of micropore and mesopore.

### 3.5. Polarized Charge density distribution on the PEME surface

Fig. 7 shows the structure of neutral PEME that is a polyelectrolyte carrying two carboxyl groups and a guanidine N-1 on the pterin ring. Six single-charged anions and cations were also studied. The charged groups were selected after identifying the main proton donor and acceptor centres in the PEME structure. The anion structures of PEME were obtained by removing a proton from donor centres (Hd-1, 2, 3, 4, 5, 6) shown in Fig. 8, whereas the cation structures were gotten by attaching a proton to the acceptor centres (Ha-1, 2, 3, 4, 5, 6) displayed in Fig. 9.

PEME exhibits a surface with groups charged differently in Fig. 10. Molecular fragments determined by the aromatic rings, distinguished by yellow-green colors composed of highly polarizable electron structures able to participate in dispersive and van der Waals interactions, and to show a certain capacity for  $\pi$ - $\pi$  stacking interaction with the AC supported by the extended  $\pi$ -electron cloud associated to the conjugated rings. Beyond that, regions colored in dark red and dark blue correspond to molecular fragments having high capacity to accept and donate protons, respectively. Carboxylic and hydroxyl oxygen atoms are negatively polarized, and consequently may act as good proton acceptors. H atoms

bonded to O and N ones are positively polarized and could be donated in acid–base interactions. It is important to note that not only the –OH and –NH<sub>2</sub> protons have certain acid character, but also those attached to the N belonging to the five– and six–membered conjugated rings. This implies a strong amphoteric character due to the proton acceptor and proton donor centres distributed over all molecules. Since H–bond interactions are stronger than dispersive and van der Waals ones, the peculiar electronic structure of PEME opens possibilities to interact not only with the AC but also with water molecules of aqueous media, and additionally to interact with itself. Thus, the complete set of all possible interactions related to the adsorption of PEME on the ACs surface from aqueous solutions allows hypothesized that this phenomenon has a complex nature with possible different orientations of the adsorbate with respect to the substrate, as well as the possibility to do mono– and multi–layer adsorptions (by the self–aggregation of the PEME molecules).

However, such competition should be less if ACs are functionalized with groups able to interact with PEME. Matos et al. showed that phosphate groups had a significant influence on the adsorption of methylene blue onto carbon–supported P–promoted Fe–based photocatalysts [42]. In our case, infrared spectroscopy (Fig. 2) and the O/C ratio (Table 2) showed that both AC2 and AC3 contained more oxygenated groups such as acid, lactone or phosphate than AC1, which could explain to a higher trend to do monolayer adsorption. These theoretical results agree well with the experimental results obtained in previous sections. Thus, equilibrium data of AC3 and AC2 are well fitted to Langmuir isotherm which considers the occurrence of a monolayer adsorption as main assumption.

The pK<sub>a</sub> values of PEME are shown in Table 6. As a rule, the more stable is the PEME anion, the lower is the pK<sub>a</sub> and the higher is the  $K_{eq}$ . Inverse to the scale of the acid pK<sub>a</sub>, for base pK<sub>a</sub> scale, a large value indicates a strong base, whereas a small or negative value indicates a weak base or no base at all. Based on the pK<sub>a</sub> results of PEME species, one can

suggest that protons of the carboxylic groups (Hd-1 and Hd-2) have the biggest acidic character followed by the proton bonded to the N belonging (Hd-5) to the six-membered ring. In addition, the N belongs to the six-membered ring (Ha-5) and the carbonyl oxygen bonded to the same ring (Ha-4) seem to be the strongest proton-acceptor centres in the PEME molecule.

### 3.6. *Effect of solution pH*

The adsorption capacities in terms of different initial pH are presented in Fig. 11. It can be seen that the adsorption capacity decreased from 208 to 85 mg.g<sup>-1</sup> for AC1, from 246 to 50 mg.g<sup>-1</sup> for AC2, and from 247 to 98 mg.g<sup>-1</sup> for AC3 while the pH increased from 3 to 10. According to the acidic and basic pKa values listed in Table 6, it may be possible to make the PEME ionic form relatively stable in the aqueous system at pH 5.4, 5.9, 6.8 for anions formation, and 6.0, 8.4 for cations formation. On the basis of pKa values obtained above, the charge distribution of PEME and ACs as a function of the pH is proposed and listed in Table 7.

At a pH value less than 3.6, the ACs surfaces are mainly dominated by positive charges as shown from the Zeta potential measurements (Fig. 1), AC3 having the highest positive charge. In the range of pH from 3.6 to 4.5, both AC1 and AC2 are more and more negatively charged, while AC3 remains positively charged. The surfaces of ACs are mainly occupied by negative charges. The number of charges increases at pH values greater than 4.5. Specifically, AC2 bears the highest negative values which is associated to the presence of hydroxyl and carboxylate groups on its surface (cf. Fig 2). For pH values below 5.4, PEME mainly carries two positive charges, since the -N and =O functional groups belonging to the six-membered ring can acquire a proton. At pH values ranging from 5.4 to 5.9, PEME behaves as a zwitterion with an additional negative charge due to the loss of a proton (Hd-1) coming from

one carboxylic functional group. As the pH increases in the range from 6.0 to 6.8, PEME molecule continues to get a negative charge from another  $\text{-COO}^-$  (Hd-2), but loses an extraneous  $\text{H}^+$  (Ha-4) attached to  $=\text{O}$  of the six-membered ring, and then exhibits a form with two negative charges and one positive charge. Once the pH value rises between 6.8–8.4, PEME will gain one more negative charge because of the separation of the proton (Hd-5) from the bound N. At a pH higher than 8.4, three negative charges appear as a result of the  $\text{H}^+$  (Ha-5) loss; the ACs surfaces are also mainly occupied by negative charges.

At higher pH values, the electrostatic repulsive force generated by the same negative charges between PEME and ACs must reduce the adsorption affinity, hindering the adsorption capability of the adsorbent. In addition, if PEME and the three ACs have the same positive charge with a repelling electrostatic force at a pH below 3.5, the affinity of PEME by ACs is higher compared to that observed at other pH values. To explain this phenomenon, we could assume that interactions can occur by  $\pi$ - $\pi$  stacking interactions on the portion of PEME which is not charged, but also we have to take into account that even if AC is positively charged, it remains regions of the surface which are negatively charged for which H bonds between PEME and ACs can generate.

### 3.7. Raman analysis

Tuinstra and Koenig firstly reported the Raman spectra of graphite fiber surfaces in 1970 [43]. Since then, Raman spectroscopy has proved to be a useful method for characterizing graphite in previous studies [44,45]. Fig. 12 shows the Raman spectra of ACs before and after PEME adsorption.

Raman spectra exhibit two sharp bands at about  $1350\text{ cm}^{-1}$  and  $1595\text{ cm}^{-1}$ , assigned to D-band and G-band, respectively, and one broad peak at approximately  $2500\text{--}3200\text{ cm}^{-1}$  caused either by the presence of either OH group of carboxylic acid or disordered substances

[46]. D-band is Raman active whenever a disorder is presented by imperfections or loss of hexagonal symmetry in the carbon structure [47] while G-band originates from the C–C band stretching vibration of graphite domains [48].

The graphitization degree values of the three ACs before (fresh) and after (used) adsorption of PEME are listed in Table 8. Obviously, it can be found that the  $R_{\text{fresh}}$  value of AC1 is 1.10, which is the largest one among the three ACs, indicating that AC1 had the lowest degree of graphitization. After PEME adsorption, all the  $R_{\text{used}}$  values increased, indicating that the graphitization degree of ACs decreased. Indeed,  $R$  is a measure of the  $\text{sp}^2$  ring clusters in a network of  $\text{sp}^2$  and  $\text{sp}^3$  bonded carbon [49,50]. The decrease in the degree of graphitization can be associated to a loss of the  $\text{sp}^2$  character of the C–C bonds due to the interaction of the adsorbate with the adsorbent. An axial interaction of PEME with ACs should displace the carbons of the latter out from the plane of the conjugated structure, thus correspondingly “breaking” the  $\text{sp}^2$  symmetry of the carbons in the carbonous skeleton. Then the results of  $R_{\text{used}} - R_{\text{fresh}}$  suggest that interactions of PEME with ACs distort more the  $\text{sp}^2$  symmetry in the sequence: AC3 (0.03) > AC2 (0.02) > AC1 (0.01).

Since  $\pi$ - $\pi$  interactions between PEME and ACs seem not to be predominant (a high  $\pi$ - $\pi$  interaction level should decrease  $R$  value because the conjugated structure obtained should be reinforced), we can suppose, in line with COSMO results, that interactions between PEME and AC2/AC3 are mainly directionally specific and can include H-bond, dipole-dipole or ionic interactions explaining a monolayer adsorption preference. On contrary, AC1 being the less oxidized, it is more favourable to do multilayers adsorption (because of PEME self-aggregation) with respect to the solid surface involving further  $\pi$ - $\pi$  interactions.

#### 4. Conclusions

This is the first systematic study on the removal of PEME from water by adsorption. For this purpose, three ACs obtained from wood and activated either by steam (AC1) or phosphoric acid (AC2 and AC3) were characterized. In addition, the adsorption mechanism of PEME with the materials tested was tentatively explained. The results showed that experimental data obtained with AC1 and AC3 were better described by the Freundlich and Langmuir models, respectively, whereas both Freundlich and Langmuir models could be used with AC2. Furthermore, both physical and chemical adsorption may exist in all ACs since the adsorption process mainly obeyed models of Dubinin–Radushkevich, pseudo–second–order and Elovich.

The polarized charge distribution of PEME showed a series of potential adsorption mechanisms, such as  $\pi$ - $\pi$  stacking, H–bond, acid–base, dispersive and van der Waals interactions, which would indicate that the molecule could interact onto the ACs surface by different ways but also with itself. As a consequence, different orientations of the adsorbate with the adsorbent surface can generate, either a preference for a multilayer adsorption or a monolayer if AC is functionalized with groups able to interact strongly with PEME. Fitting procedure demonstrated that both AC2 and AC3 can be fitted to the Langmuir isotherm. These findings were consistent with DRIFTS analysis and O/C ratios, in which AC3 and AC2 containing more oxygenated groups are further prone to a monolayer adsorption mechanism. Raman spectroscopy showed a reduction of the graphitization degree of ACs after interactions with PEME, more particularly for the carbons activated by phosphoric acid, indicating that  $\pi$ - $\pi$  interactions were not predominant.

Although some interesting results have been obtained, further work needs to be performed to envisage industrial applications, such as adsorptive experiments in aqueous solutions containing ionic species and dissolved organic matters, as well as to define a continuous adsorption process. Additionally, it is important to explore different strategies for



the adsorbent regeneration and reuse which could include desorption (i.e., thermal and non-thermal technologies) and decomposition (i.e., electrochemistry, microbiological, chemical and ultrasound methods).

## **Acknowledgements**

Authors gratefully acknowledge the contribution of the China Scholarship Council in supporting a doctoral thesis study for Bomin FU. The authors are also very grateful to Université Claude Bernard Lyon 1, Centre National de la Recherche Scientifique, Institut de Recherches sur la Catalyse et l'Environnement de Lyon (IRCELYON) for their financial support. In particular, the authors would like to thank the IRCELYON for its technical services such as Raman, physical and chemical analysis on this work. The authors also thank the Centro de Computación Científica at the Universidad Autónoma de Madrid for the computational support to this work.

## **References**

- [1] C. Sophia, E.C. Lima, Removal of emerging contaminants from the environment by adsorption, *Ecotoxicol. Environ. Saf.* 150 (2018) 1–17.
- [2] J. Martín, M. del Mar Orta, S. Medina–Carrasco, J.L. Santos, I. Aparicio, E. Alonso, Removal of priority and emerging pollutants from aqueous media by adsorption onto synthetic organo–functionalized high–charge swelling micas, *Environ. Res.* 164 (2018) 488–494.

- [3] H.-C. Tao, H.-R. Zhang, J.-B. Li, W.-Y. Ding, Biomass based activated carbon obtained from sludge and sugarcane bagasse for removing lead ion from wastewater, *Bioresour. Technol.* 192 (2015) 611–617.
- [4] H. Karunarathne, B. Amarasinghe, Fixed bed adsorption column studies for the removal of aqueous phenol from activated carbon prepared from sugarcane bagasse, *Energy Procedia.* 34 (2013) 83–90.
- [5] S. Hokkanen, A. Bhatnagar, M. Sillanpää, A review on modification methods to cellulose-based adsorbents to improve adsorption capacity, *Water Res.* 91 (2016) 156–173.
- [6] M.J. Ahmed, Adsorption of quinolone, tetracycline, and penicillin antibiotics from aqueous solution using activated carbons: Review, *Environ. Toxicol. Pharmacol.* 50 (2017) 1–10.
- [7] J. Matos, P.S. Poon, R. Montaña, R. Romero, G.R. Gonçalves, M.A. Schettino Jr, E.C. Passamani, J.C.C. Freitas, Photocatalytic activity of P-Fe/activated carbon nanocomposites under artificial solar irradiation, *Catal. Today.* (2019).
- [8] G. Crini, E. Lichtfouse, L.D. Wilson, N. Morin-Crini, Conventional and non-conventional adsorbents for wastewater treatment, *Environ. Chem. Lett.* 17 (2019) 195–213.
- [9] M. El Gamal, H.A. Mousa, M.H. El-Naas, R. Zacharia, S. Judd, Bio-regeneration of activated carbon: a comprehensive review, *Sep. Purif. Technol.* 197 (2018) 345–359.
- [10] R. Baccar, M. Sarrà, J. Bouzid, M. Feki, P. Blázquez, Removal of pharmaceutical compounds by activated carbon prepared from agricultural by-product, *Chem. Eng. J.* 211 (2012) 310–317.

- [11] S.H. Kim, H.K. Shon, H.H. Ngo, Adsorption characteristics of antibiotics trimethoprim on powdered and granular activated carbon, *J. Ind. Eng. Chem.* 16 (2010) 344–349.
- [12] S. Kleywegt, V. Pileggi, P. Yang, C. Hao, X. Zhao, C. Rocks, S. Thach, P. Cheung, B. Whitehead, Pharmaceuticals, hormones and bisphenol A in untreated source and finished drinking water in Ontario, Canada–Occurrence and treatment efficiency, *Sci. Total Environ.* 409 (2011) 1481–1488.
- [13] K. Soni, A. Mujtaba, K. Kohli, Lipid drug conjugate nanoparticle as a potential nanocarrier for the oral delivery of pemetrexed diacid: formulation design, characterization, ex vivo, and in vivo assessment, *Int. J. Biol. Macromol.* 103 (2017) 139–151.
- [14] J.–P. Besse, J.–F. Latour, J. Garric, Anticancer drugs in surface waters: what can we say about the occurrence and environmental significance of cytotoxic, cytostatic and endocrine therapy drugs?, *Environ. Int.* 39 (2012) 73–86.
- [15] P.–H. Secrétan, M. Karoui, Y. Levi, H. Sadou–Yayé, L. Tortolano, A. Solgadi, N. Yagoubi, B. Do, Pemetrexed degradation by photocatalytic process: Kinetics, identification of transformation products and estimation of toxicity, *Sci. Total Environ.* 624 (2018) 1082–1094.
- [16] H. Li, M. Rivallan, F. Thibault–Starzyk, A. Travert, F.C. Meunier, Effective bulk and surface temperatures of the catalyst bed of FT–IR cells used for in situ and operando studies, *Phys. Chem. Chem. Phys.* 15 (2013) 7321–7327.
- [17] J. Sirita, S. Phanichphant, F.C. Meunier, Quantitative analysis of adsorbate concentrations by diffuse reflectance FT–IR, *Anal. Chem.* 79 (2007) 3912–3918.
- [18] K.Y. Foo, B.H. Hameed, Insights into the modeling of adsorption isotherm systems, *Chem. Eng. J.* 156 (2010) 2–10.

- [19] I. Khurana, A.K. Shaw, J.M. Khurana, P.K. Rai, Batch and dynamic adsorption of Eriochrome Black T from water on magnetic graphene oxide: experimental and theoretical studies, *J. Environ. Chem. Eng.* 6 (2018) 468–477.
- [20] P. Pendleton, S.H. Wu, A. Badalyan, Activated carbon oxygen content influence on water and surfactant adsorption, *J. Colloid Interface Sci.* 246 (2002) 235–240.
- [21] C.P. Amézquita–Marroquín, P. Torres–Lozada, L. Giraldo, P.D. Húmpola, E. Rivero, P.S. Poon, J. Matos, J.C. Moreno–Piraján, Sustainable production of nanoporous carbons: Kinetics and equilibrium studies in the removal of atrazine, *J. Colloid Interface Sci.* 562 (2020) 252–267.
- [22] E.G. Sogut, N. Caliskan, Isotherm and kinetic studies of Pb (II) adsorption on raw and modified diatomite by using non–linear regression method, *Fresenius Environ. Bull.* 26 (2017) 2720–2728.
- [23] Y. Liu, X. Liu, W. Dong, L. Zhang, Q. Kong, W. Wang, Efficient adsorption of sulfamethazine onto modified activated carbon: a plausible adsorption mechanism, *Sci. Rep.* 7 (2017) 1–12.
- [24] C. Peiris, S.R. Gunatilake, T.E. Mlsna, D. Mohan, M. Vithanage, Biochar based removal of antibiotic sulfonamides and tetracyclines in aquatic environments: a critical review, *Bioresour. Technol.* 246 (2017) 150–159.
- [25] P.S. Kumar, L. Korving, K.J. Keesman, M.C.M. van Loosdrecht, G.–J. Witkamp, Effect of pore size distribution and particle size of porous metal oxides on phosphate adsorption capacity and kinetics, *Chem. Eng. J.* 358 (2019) 160–169.
- [26] M. Thommes, K. Kaneko, A. V Neimark, J.P. Olivier, F. Rodríguez–Reinoso, J. Rouquerol, K.S.W. Sing, Physisorption of gases, with special reference to the evaluation of surface area and pore size distribution (IUPAC Technical Report), *Pure Appl. Chem.* 87 (2015) 1051–1069.

- [27] P. Oleszczuk, A. Zielińska, G. Cornelissen, Stabilization of sewage sludge by different biochars towards reducing freely dissolved polycyclic aromatic hydrocarbons (PAHs) content, *Bioresour. Technol.* 156 (2014) 139–145.
- [28] A. Dandekar, R.T.K. Baker, M.A. Vannice, Characterization of activated carbon, graphitized carbon fibers and synthetic diamond powder using TPD and DRIFTS, *Carbon*. 36 (1998) 1821–1831.
- [29] W. Jastrzębski, M. Sitarz, M. Rokita, K. Buat, Infrared spectroscopy of different phosphates structures, *Spectrochim. Acta, Part A*. 79 (2011) 722–727.
- [30] C. Liang, X. Zhang, P. Feng, H. Chai, Y. Huang, ZIF-67 derived hollow cobalt sulfide as superior adsorbent for effective adsorption removal of ciprofloxacin antibiotics, *Chem. Eng. J.* 344 (2018) 95–104.
- [31] M.R. Samarghandi, T.J. Al-Musawi, A. Mohseni-Bandpi, M. Zarrabi, Adsorption of cephalexin from aqueous solution using natural zeolite and zeolite coated with manganese oxide nanoparticles, *J. Mol. Liq.* 211 (2015) 431–441.
- [32] Y. Sun, Q. Yue, B. Gao, Q. Li, L. Huang, F. Yao, X. Xu, Preparation of activated carbon derived from cotton linter fibers by fused NaOH activation and its application for oxytetracycline (OTC) adsorption, *J. Colloid Interface Sci.* 368 (2012) 521–527.
- [33] T.A. Khan, S.A. Chaudhry, I. Ali, Equilibrium uptake, isotherm and kinetic studies of Cd (II) adsorption onto iron oxide activated red mud from aqueous solution, *J. Mol. Liq.* 202 (2015) 165–175.
- [34] M. Vithanage, S.S. Mayakaduwa, I. Herath, Y.S. Ok, D. Mohan, Kinetics, thermodynamics and mechanistic studies of carbofuran removal using biochars from tea waste and rice husks, *Chemosphere*. 150 (2016) 781–789.

- [35] J.L. Sotelo, G. Ovejero, A. Rodríguez, S. Álvarez, J. García, Analysis and modeling of fixed bed column operations on flumequine removal onto activated carbon: pH influence and desorption studies, *Chem. Eng. J.* 228 (2013) 102–113.
- [36] J.M. Corkill, J.F. Goodman, J.R. Tate, Adsorption of non-ionic surface-active agents at the graphon/solution interface, *Trans. Faraday Soc.* 62 (1966) 979–986.
- [37] M.A. Fontecha-Cámara, M. V López-Ramón, M.A. Álvarez-Merino, C. Moreno-Castilla, About the endothermic nature of the adsorption of the herbicide diuron from aqueous solutions on activated carbon fiber, *Carbon.* 44 (2006) 2335–2338.
- [38] Y.-S. Ho, G. McKay, Pseudo-second order model for sorption processes, *Process Biochem.* 34 (1999) 451–465.
- [39] Y. Li, M.A. Taggart, C. McKenzie, Z. Zhang, Y. Lu, S. Pap, S. Gibb, Utilizing low-cost natural waste for the removal of pharmaceuticals from water: Mechanisms, isotherms and kinetics at low concentrations, *J. Cleaner Prod.* 227 (2019) 88–97.
- [40] M. Alkan, Ö. Demirbağ, M. Doğan, Adsorption kinetics and thermodynamics of an anionic dye onto sepiolite, *Microporous Mesoporous Mater.* 101 (2007) 388–396.
- [41] T.C. Nguyen, P. Loganathan, T.V. Nguyen, S. Vigneswaran, J. Kandasamy, R. Naidu, Simultaneous adsorption of Cd, Cr, Cu, Pb, and Zn by an iron-coated Australian zeolite in batch and fixed-bed column studies, *Chem. Eng. J.* 270 (2015) 393–404.
- [42] J. Matos, J. Arcibar-Orozco, P.S. Poon, G. Pecchi, J.R. Rangel-Mendez, Influence of phosphorous upon the formation of DMPO-OH and POBN-O<sub>2</sub><sup>-</sup> spin-trapping adducts in carbon-supported P-promoted Fe-based photocatalysts, *J. Photochem. Photobiol., A.* 391 (2020) 112362.
- [43] F. Tuinstra, J.L. Koenig, Characterization of graphite fiber surfaces with Raman spectroscopy, *J. Compos. Mater.* 4 (1970) 492–499.

- [44] X. He, K.B. Male, P.N. Nesterenko, D. Brabazon, B. Paull, J.H.T. Luong, Adsorption and desorption of methylene blue on porous carbon monoliths and nanocrystalline cellulose, *ACS Appl. Mater. Interfaces*. 5 (2013) 8796–8804.
- [45] A. Reyhani, S.Z. Mortazavi, A.Z. Moshfegh, A.N. Golikand, M. Amiri, Enhanced electrochemical hydrogen storage by catalytic Fe-doped multi-walled carbon nanotubes synthesized by thermal chemical vapor deposition, *J. Power Sources*. 188 (2009) 404–410.
- [46] M. Tagliavini, F. Engel, P.G. Weidler, T. Scherer, A.I. Schäfer, Adsorption of steroid micropollutants on polymer-based spherical activated carbon (PBSAC), *J. Hazard. Mater.* 337 (2017) 126–137.
- [47] F.J. Maldonado-Hódar, C. Moreno-Castilla, J. Rivera-Utrilla, Y. Hanzawa, Y. Yamada, Catalytic graphitization of carbon aerogels by transition metals, *Langmuir*. 16 (2000) 4367–4373.
- [48] A. Jorio, M.A. Pimenta, A.G. Souza Filho, R. Saito, G. Dresselhaus, M.S. Dresselhaus, Characterizing carbon nanotube samples with resonance Raman scattering, *New J. Phys.* 5 (2003) 139.
- [49] M. Chhowalla, A.C. Ferrari, J. Robertson, G.A.J. Amaratunga, Evolution of sp<sup>2</sup> bonding with deposition temperature in tetrahedral amorphous carbon studied by Raman spectroscopy, *Applied Physics Letters*. 76 (2000) 1419–1421.
- [50] C. Mattevi, G. Eda, S. Agnoli, S. Miller, K.A. Mkhoyan, O. Celik, D. Mastrogiovanni, G. Granozzi, E. Garfunkel, M. Chhowalla, Evolution of electrical, chemical, and structural properties of transparent and conducting chemically derived graphene thin films, *Adv. Funct. Mater.* 19 (2009) 2577–2583.

**Table captions:**

**Table 1.** Textural properties of ACs.

**Table 2.** The mass percentage of total C, O, H, N, S and atomic ratios in ACs.

**Table 3.** The percentage contents of other elements in ACs determined by ICP–OES.

**Table 4.** Isotherm parameters for PEME sorption onto ACs at different temperatures.

**Table 5.** Kinetic parameters of ACs.

**Table 6.** Acid and base pKa values of PEME calculated by COSMO–RS.

**Table 7.** Charge distributions of PEME and ACs at different pH values.

**Table 8.** Graphitization degree of ACs before and after adsorption of PEME.

**Figure captions:**

**Fig. 1.** Zeta potentials of ACs under different pH conditions.

**Fig. 2.** DRIFTS spectra of ACs. The spectra were collected at 100°C under 20 mL/min He. The signal of KBr was used as the background.

**Fig. 3.** Effect of adsorbent dose on the removal rate of PEME. Experimental conditions: 10 mg. L<sup>-1</sup> PEME, temperature = 25 °C, initial solution pH = 6, contact time = 24h.

**Fig. 4.** Adsorption capacities ( $q_e$ ) of AC1 (a), AC2 (b) and AC3 (c) for PEME ( $C_e$ ) at different temperatures. Experimental conditions: 2, 5, 10, 15, 20 mg. L<sup>-1</sup> PEME, 0.0375 g. L<sup>-1</sup> ACs, initial solution pH = 6, contact time = 48h.

**Fig. 5.** Adsorptive capacities ( $q_t$ ) of PEME onto ACs at different times ( $t$ ). Experimental conditions: 10 mg. L<sup>-1</sup> PEME, 0.0375 g. L<sup>-1</sup> ACs, temperature = 25 °C, initial solution pH = 6.

**Fig. 6.** The Weber–Morris plot of PEME on ACs.

**Fig. 7.** Two–dimensional (a) and optimal three–dimensional structures (b) of neutral PEME.

**Fig. 8.** Proton donor centres considered in anions formation of PEME.



**Fig. 9.** Proton acceptor centres considered in cations formation of PEME.

**Fig. 10.** Three different views of polarized charge density distribution on the molecular surface of PEME established by COSMO.

**Fig. 11.** The effects of pH on the equilibrium adsorption capacities ( $q_e$ ) of PEME by ACs. Experimental conditions: 10 mg. L<sup>-1</sup> PEME, 0.0375 g. L<sup>-1</sup> ACs, temperature = 25 °C, contact time = 48h.

**Fig. 12.** Raman spectra of AC1 (a), AC2 (b) and AC3 (c) before and after PEME adsorption.

**Table 1**

Textural properties of ACs.

Adsorbent	$S_{\text{BET}}^{\text{a}}$ ( $\text{m}^2.\text{g}^{-1}$ )	$S_{\text{micro}}^{\text{b}}$ ( $\text{m}^2.\text{g}^{-1}$ )	$V_{\text{micro}}^{\text{c}}$ ( $\text{cm}^3.\text{g}^{-1}$ )	$V_{\text{meso}}^{\text{d}}$ ( $\text{cm}^3.\text{g}^{-1}$ )	$W_{\text{micro}}^{\text{e}}$ (nm)	$D_{\text{meso}}^{\text{f}}$ (nm)
AC1	855	765	0.32	0.10	0.80	4.39
AC2	1293	844	0.39	0.80	1.18	4.87
AC3	1721	994	0.51	1.30	1.26	4.93

<sup>a</sup> Total BET surface area; <sup>b</sup> micropore surface area; <sup>c</sup> microporous volume; <sup>d</sup> mesoporous volume; <sup>e</sup> median pore width; <sup>f</sup> average pore diameter.

**Table 2**

The mass percentage of total C, O, H, N, S and atomic ratios in ACs.

Adsorbent	C (%)	O (%)	H (%)	N (%)	S (%)	O/C	(O+N)/C
AC1	86.3	5.7	1.0	0.4	0.2	0.07	0.07
AC2	80.2	11.1	3.1	0.3	0.1	0.14	0.14
AC3	76.2	10.5	2.4	0.5	0.2	0.14	0.15

**Table 3**

The percentage contents of other elements in ACs determined by ICP–OES.

Adsorbent	P (%)	Fe (%)	Ca (%)	Na (%)	Al (%)	Mg (%)	K (%)	Mo (%)	Mn (%)	Zn (%)	Ba (%)	Si (%)
AC1	0.1	0.1	1.5	0.2	0.2	0.2	0.9	<0.05	<0.05	<0.05	<0.05	0.61
AC2	1.4	0.01	0.1	<0.05	<0.05	<0.05	0.05	<0.05	<0.05	<0.05	<0.05	<0.01
AC3	1.3	0.1	0.1	<0.05	0.13	<0.05	0.05	<0.05	<0.05	<0.05	<0.05	0.50

Note: Ag, As, Cd, Co, Cr, Cu, Ni, Pb, Sb, Se, Ti, Tl, V, Zr, Sr, Te, Bi, Ga, In, Ta, Hf <<< 0.05%

**Table 4**

Isotherm parameters for PEME sorption onto ACs at different temperatures.

Activated carbon	Temperature (°C)	Freundlich			Langmuir			Dubinin–Radushkevich			
		$K_F$ (L.g <sup>-1</sup> )	$n$	$R^2$	$K_L$ (L.mg <sup>-1</sup> )	$q_m$ (mg.g <sup>-1</sup> )	$R^2$	$K_D$ (mol <sup>2</sup> .kJ <sup>-2</sup> )	$q_{mD}$ (mg.g <sup>-1</sup> )	$E$ (kJ.mol <sup>-1</sup> )	$R^2$
AC1	10	51.8	5.43	0.9936	3.24	80	0.9357	0.050	77	3.2	0.9141
	15	52.2	4.86	0.9999	1.92	88	0.9662	0.074	82	2.6	0.9368
	20	67.2	5.29	0.9967	3.17	105	0.9706	0.043	100	3.4	0.9494
	25	78.3	3.92	0.9943	1.65	145	0.9376	0.046	129	3.3	0.8893
	35	78.3	3.79	0.9928	1.47	150	0.9366	0.046	132	3.3	0.8836
AC2	10	87.7	4.21	0.9723	1.67	159	0.9941	0.088	145	2.4	0.9729
	15	87.2	3.84	0.9862	1.43	167	0.9806	0.077	148	2.5	0.9343
	20	102.4	4.10	0.9670	2.01	183	0.9848	0.072	170	2.6	0.9743
	25	107.1	3.51	0.9805	1.44	211	0.9881	0.086	190	2.4	0.9603
	35	108.1	3.28	0.9858	1.31	222	0.9800	0.084	197	2.4	0.9446
AC3	10	147.4	3.98	0.9084	2.40	255	0.9290	0.059	237	2.9	0.9158
	15	153.3	3.39	0.9164	2.41	266	0.9571	0.058	247	2.9	0.9538
	20	161.6	3.81	0.9173	2.36	282	0.9547	0.054	259	3.0	0.9464
	25	181.4	3.56	0.9070	2.06	324	0.9579	0.056	291	3.0	0.9453
	35	190.0	3.57	0.8950	2.08	338	0.9583	0.054	303	3.0	0.9499

**Table 5**

Kinetic parameters of ACs.

Activated carbon	Pseudo–first–order			Pseudo–second–order			Elovich		Intra–particle diffusion			
	$q_e$ (mg.g <sup>-1</sup> )	$k_1$ (h <sup>-1</sup> )	$R^2$	$q_e$ (mg.g <sup>-1</sup> )	$k_2$ (g.(mg.h) <sup>-1</sup> )	$R^2$	$\square$ (mg.(g.h) <sup>-1</sup> )	$\square$ (g.mg <sup>-1</sup> )	$R^2$	$k_d$ (mg.(g.h <sup>0.5</sup> ) <sup>-1</sup> )	$C$ (mg.g <sup>-1</sup> )	$R^2$
AC1	88	1.95	0.7530	94	0.026	0.8534	$1.33 \times 10^3$	0.08	0.9734	10.0	46	0.9699
AC2	144	1.96	0.8545	152	0.017	0.9944	$2.52 \times 10^3$	0.05	0.9925	12.9	90	0.9826
AC3	207	6.71	0.9074	214	0.050	0.9524	$5.99 \times 10^5$	0.06	0.9753	11.5	166	0.9926

**Table 6**

Acid and base pKa values of PEME calculated by COSMO-RS.

Specie	Centre	pKa	$K_{eq}$
PEME	Hd-1	5.4	$3.98 \times 10^{-6}$
	Hd-2	5.9	$1.26 \times 10^{-6}$
	Hd-3	15.4	$3.98 \times 10^{-16}$
	Hd-4	11.3	$5.01 \times 10^{-12}$
	Hd-5	6.8	$1.58 \times 10^{-7}$
	Hd-6	14.5	$3.16 \times 10^{-15}$
PEME <sup>+</sup>	Ha-1	-8.7	$2.00 \times 10^{-23}$
	Ha-2	-8.5	$3.16 \times 10^{-23}$
	Ha-3	-3.2	$6.31 \times 10^{-18}$
	Ha-4	6.0	$1.00 \times 10^{-8}$
	Ha-5	8.4	$2.51 \times 10^{-6}$
	Ha-6	-2.9	$1.26 \times 10^{-17}$

**Table 7**

Charge distributions of PEME and ACs at different pH values.

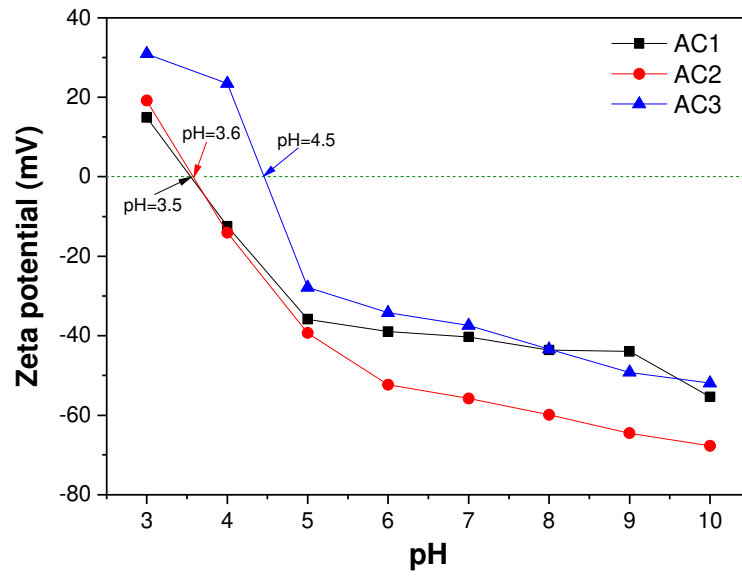
pH range	PEME charge (estimation)	AC1 charge (pHpzc =3.5)	AC2 charge (pHpzc =3.6)	AC3 charge (pHpzc =4.5)
<3.6	+, +	++	++	++
3.6–4.5	+, +			++
4.5–5.4	+, +			
5.4–5.9	+, +,			

6.0–6.8	+, ,
6.8–8.4	+, , ,
>8.4	, ,

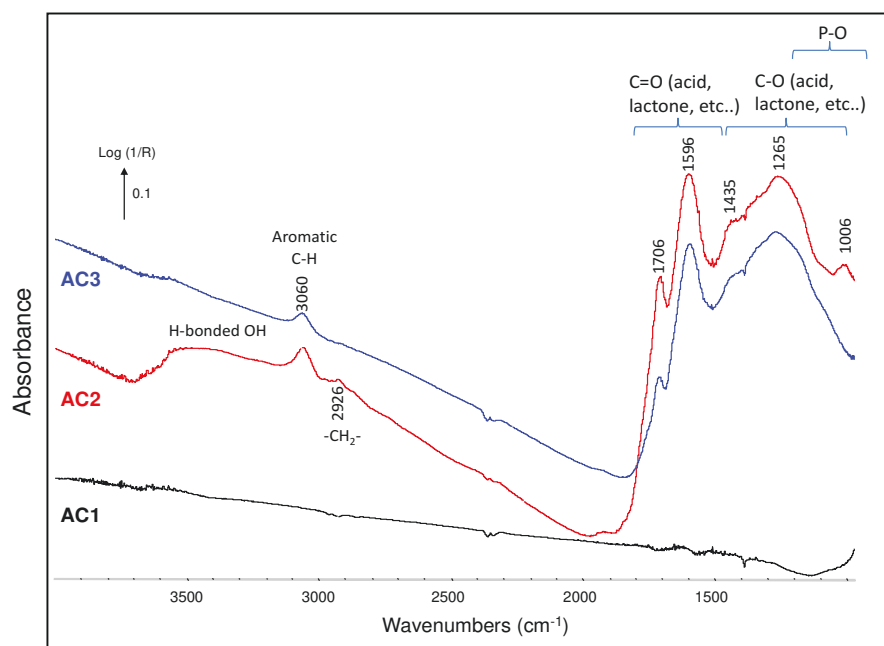
**Table 8**

Graphitization degree of ACs before and after adsorption of PEME.

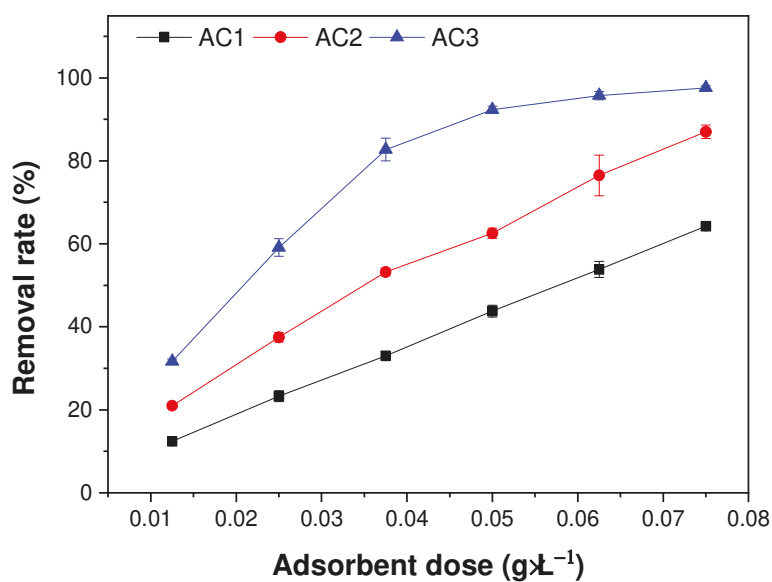
Adsorbent	$R_{\text{fresh}}$	$R_{\text{used}}$	$R_{\text{used}} - R_{\text{fresh}}$
AC1	1.10	1.11	0.01
AC2	0.80	0.82	0.02
AC3	0.80	0.83	0.03



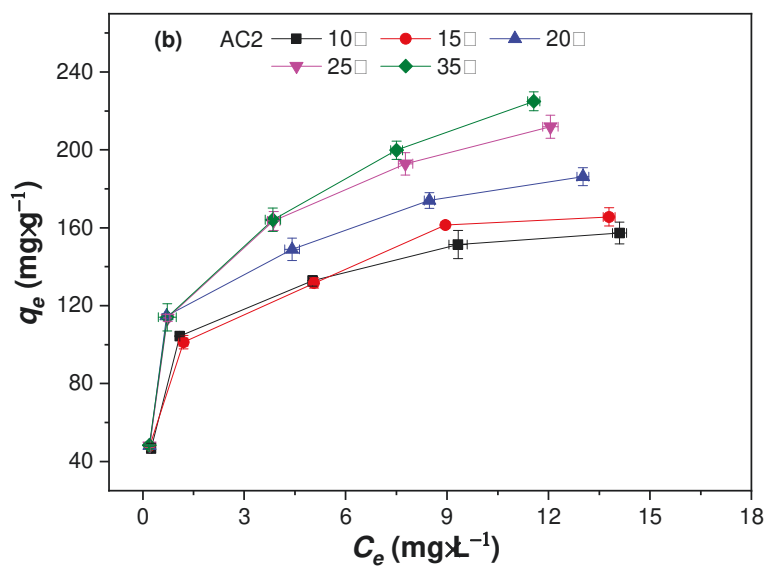
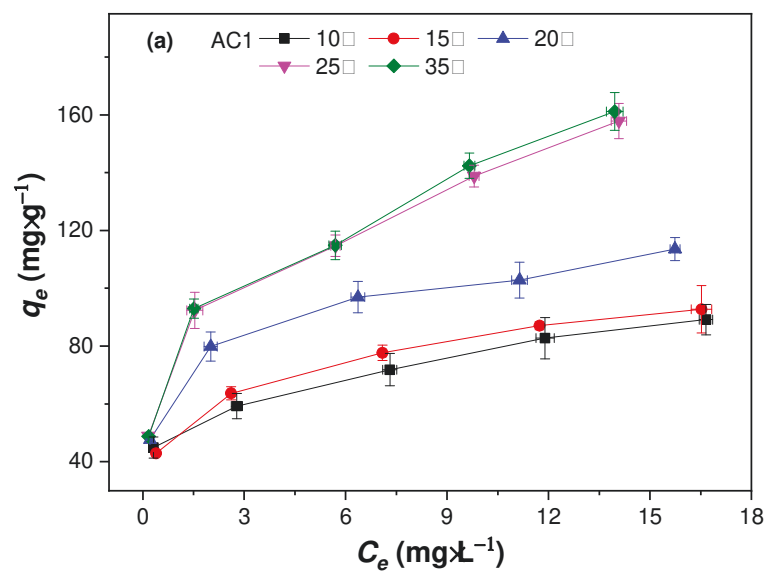
**Fig. 1.** Zeta potentials of ACs under different pH conditions.

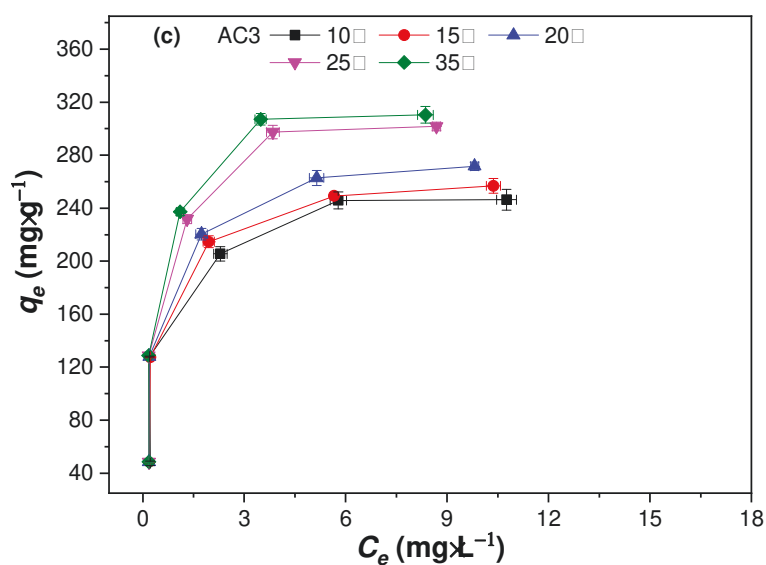


**Fig. 2.** DRIFTS spectra of ACs. The spectra were collected at 100°C under 20 mL.min<sup>-1</sup> He. The signal of KBr was used as the background.

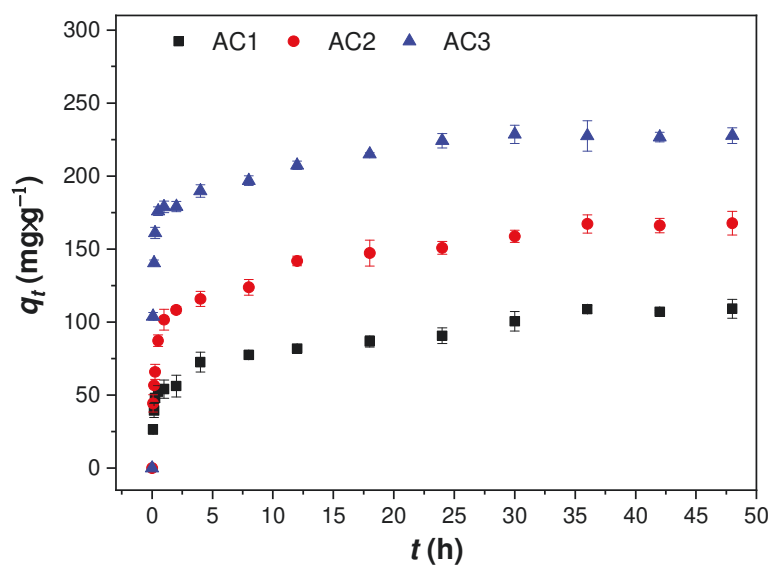


**Fig. 3.** Effect of adsorbent dose on the removal rate of PEME. Experimental conditions: 10 mg.L<sup>-1</sup> PEME, temperature = 25 °C, initial solution pH = 6, contact time = 24h.



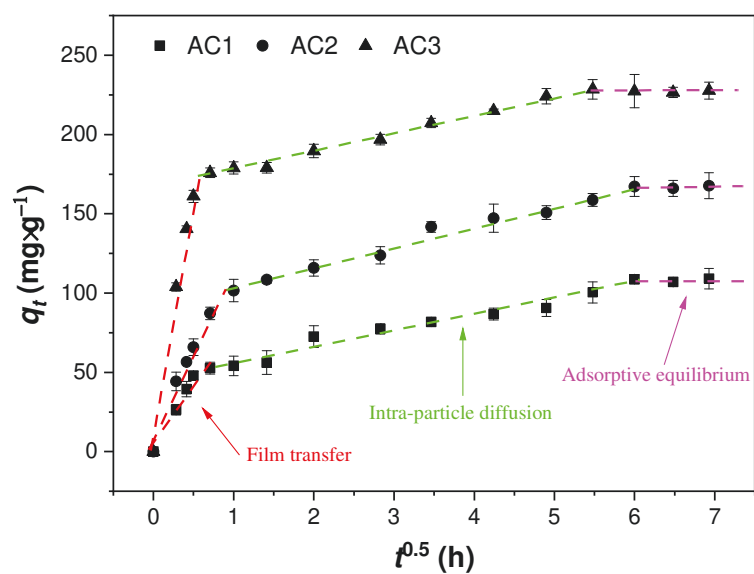


**Fig. 4.** Adsorption capacities ( $q_e$ ) of AC1 (a), AC2 (b) and AC3 (c) for PEME ( $C_e$ ) at different temperatures. Experimental conditions: 2, 5, 10, 15, 20 mg·L<sup>-1</sup> PEME, 0.0375 g·L<sup>-1</sup> ACs, initial solution pH = 6, contact time = 48h.

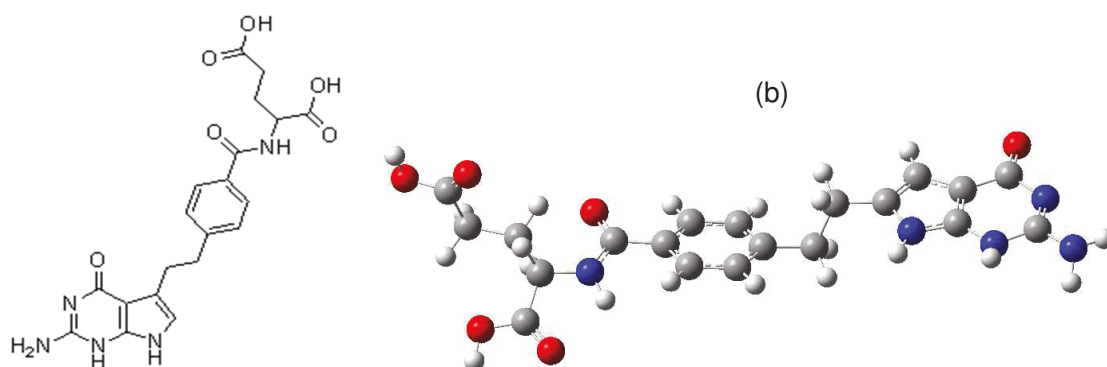


**Fig. 5.** Adsorptive capacities ( $q_t$ ) of PEME onto ACs at different times ( $t$ ). Experimental conditions: 10 mg·L<sup>-1</sup> PEME, 0.0375 g·L<sup>-1</sup> ACs, temperature = 25 °C, initial solution pH = 6.

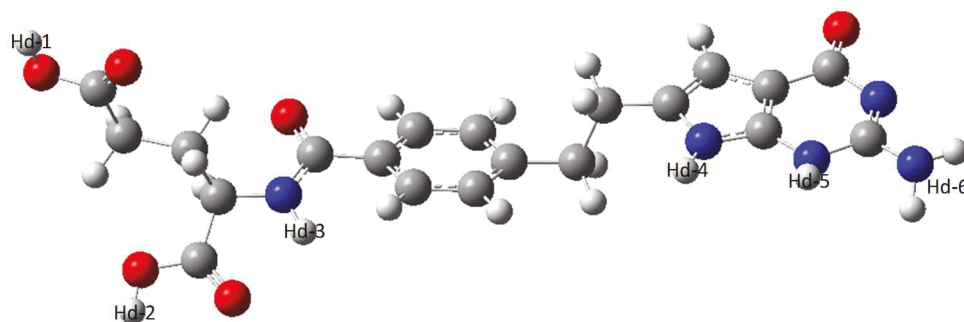




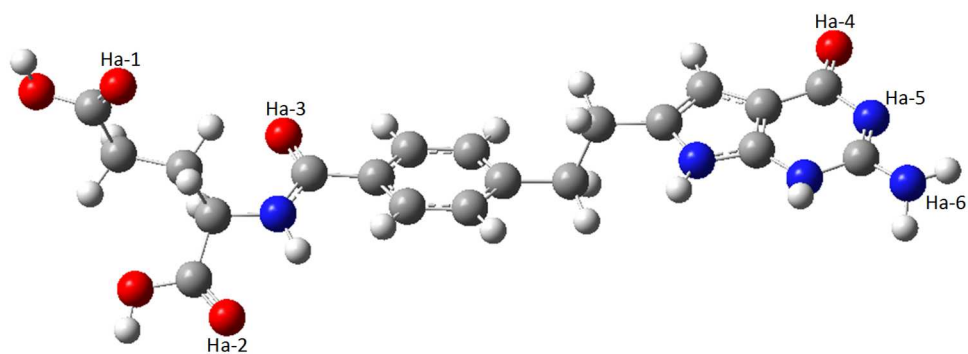
**Fig. 6.** The Weber–Morris plot of PEME on ACs.



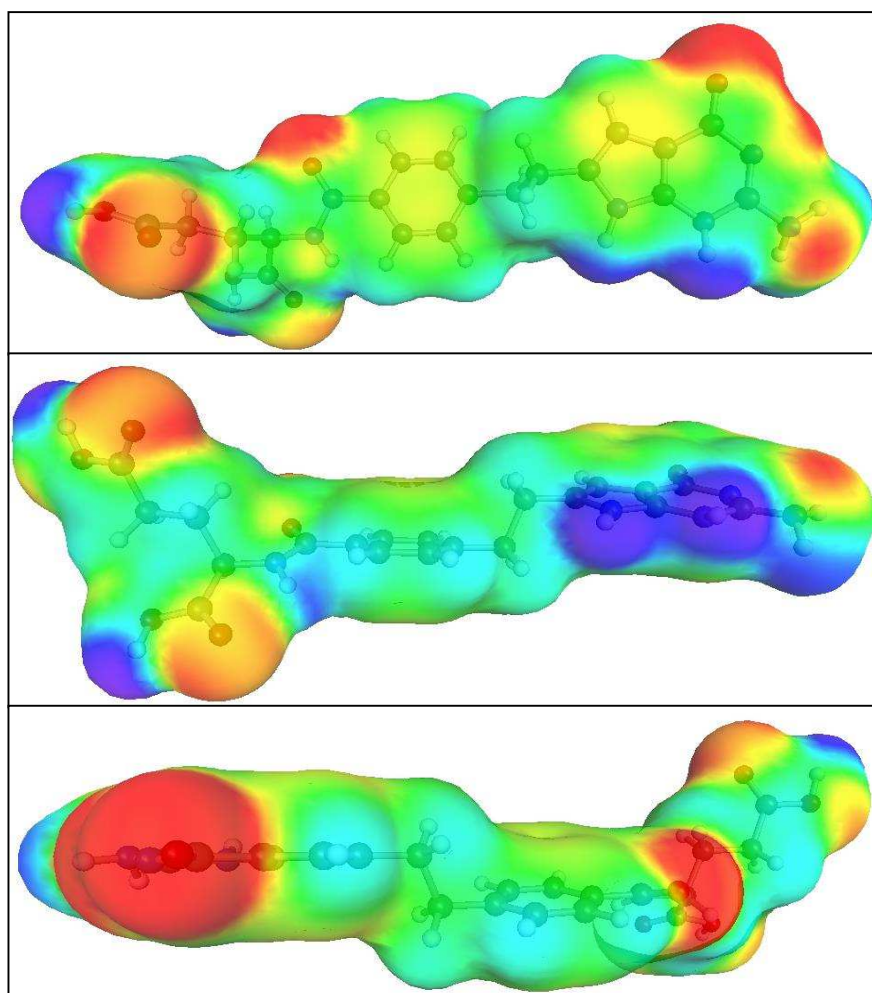
**Fig. 7.** Two-dimensional (a) and optimal three-dimensional structures (b) of neutral PEME.



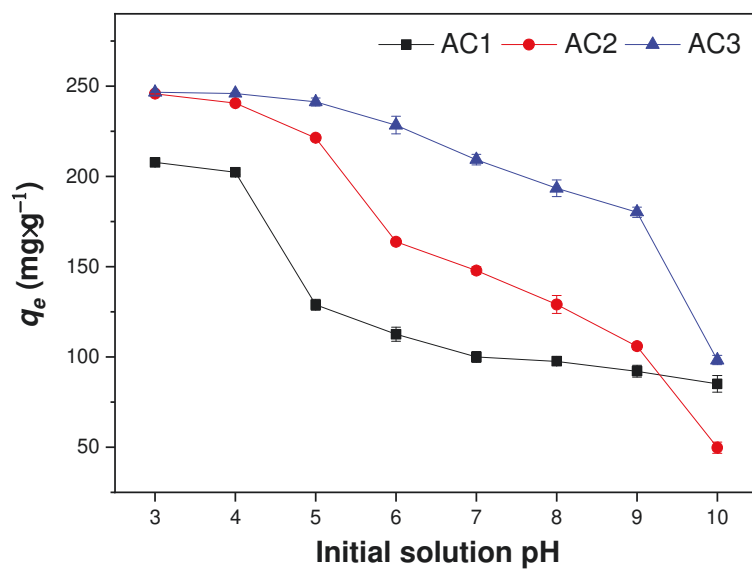
**Fig. 8.** Proton donor centres considered in anions formation of PEME.



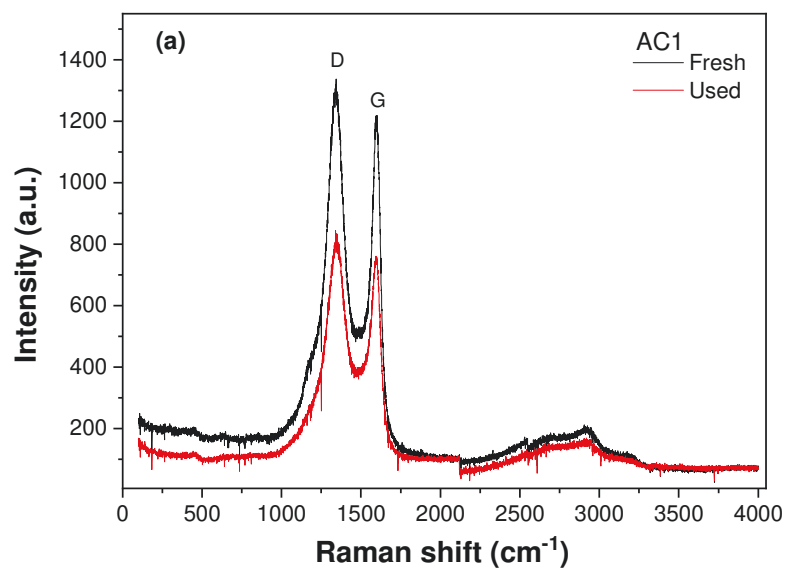
**Fig. 9.** Proton acceptor centres considered in cations formation of PEME.



**Fig. 10.** Different angled views of polarized charge density distribution on the molecular surface of PEME established by COSMO.



**Fig. 11.** The effects of pH on the equilibrium adsorption capacities ( $q_e$ ) of PEME by ACs. Experimental conditions: 10 mg·L<sup>-1</sup> PEME, 0.0375 g·L<sup>-1</sup> ACs, temperature = 25 °C, contact time = 48h.



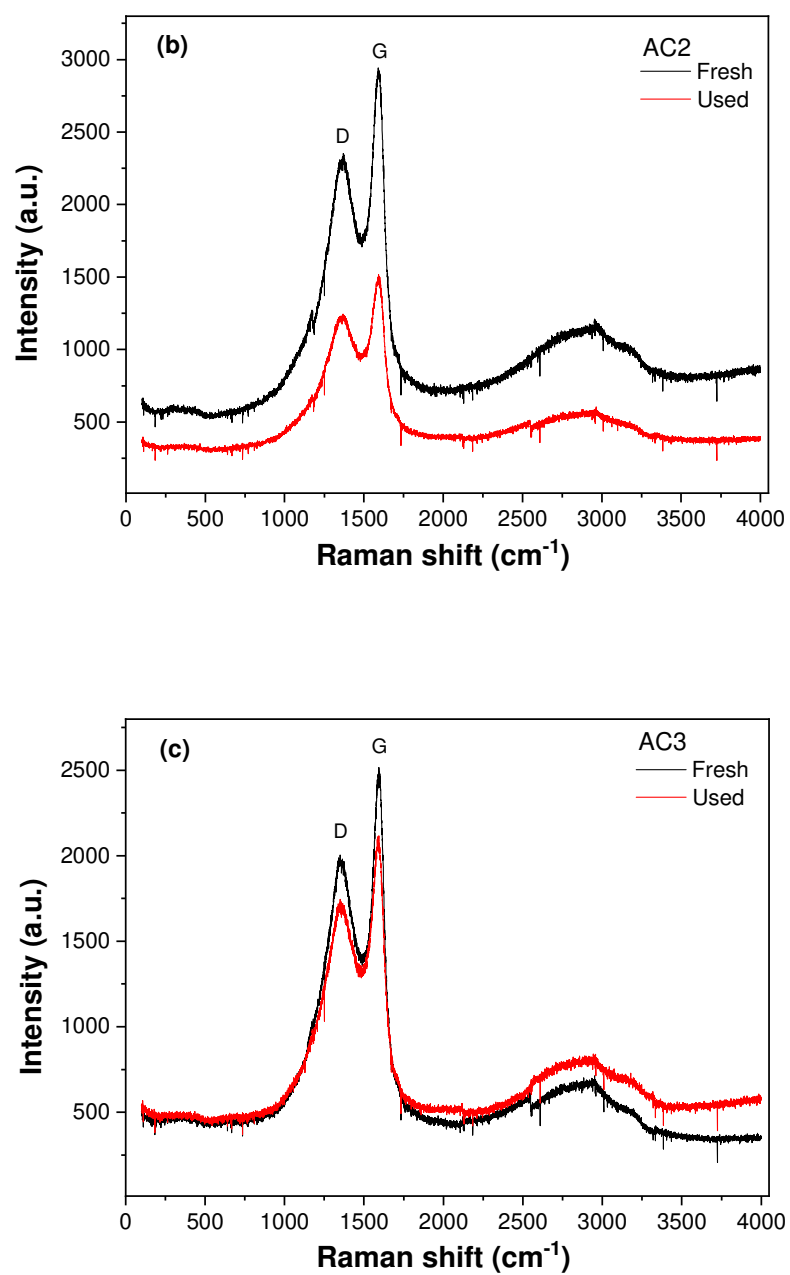


**Fig. 12.** Raman spectra of AC1 (a), AC2 (b) and AC3 (c) before and after PEME adsorption.